

# Continuous aridification since the mid-Holocene as the main cause of C<sub>3</sub>/C<sub>4</sub> dynamics in the grasslands of northeastern China

Nannan Li<sup>1,2,3,4</sup>  | Manman Xie<sup>5</sup> | Dorothy Sack<sup>6</sup> | Nathalie Dubois<sup>4,7</sup> |  
Xiuyun Yang<sup>8</sup> | Guizai Gao<sup>1</sup> | Dehui Li<sup>1</sup> | Lidan Liu<sup>9</sup> | Hongyan Liu<sup>10</sup> |  
Chengcheng Leng<sup>1</sup> | Jiangyong Wang<sup>1</sup> | Baojian Liu<sup>11</sup> | Dongmei Jie<sup>1,2,12</sup> 

<sup>1</sup>Institute for Peat and Mire Research, State Environmental Protection Key Laboratory of Wetland Ecology and Vegetation Restoration, Northeast Normal University, Changchun, China

<sup>2</sup>School of Geographical Sciences, Northeast Normal University, Changchun, China

<sup>3</sup>CEREGE, CNRS, IRD, INRA, Aix-Marseille University, Europôle de l'Arbois, Aix-en-Provence, France

<sup>4</sup>Surface Waters – Research and Management, Eawag, Swiss Federal Institute of Aquatic Science and Technology, Dübendorf, Switzerland

<sup>5</sup>National Research Center for Geoanalysis, Chinese Academy of Geological Sciences, Beijing, China

<sup>6</sup>Department of Geography, Ohio University, Athens, Ohio

<sup>7</sup>Department of Earth Sciences, ETH Zürich, Zürich, Switzerland

<sup>8</sup>College of Urban and Environmental Science, Peking University, Beijing, China

<sup>9</sup>College of Resource and Environment Science, Hunan Normal University, Changsha, China

<sup>10</sup>School of Resources Environment and Tourism, Anyang Normal University, Anyang, China

<sup>11</sup>School of Life Science, Jilin Normal University, Siping, China

<sup>12</sup>Key Laboratory of Vegetation Ecology, Ministry of Education, Changchun, China

## Correspondence

Dongmei Jie, School of Geographical Sciences, Northeast Normal University, No. 5268, Renmin Street, Changchun 130024, Jilin, China.  
Email: jiedongmei@nenu.edu.cn

## Funding information

National Natural Science Foundation of China, Grant/Award Numbers: 41471164, 41771214, 41971100; National Key Research and Development Project of China, Grant/Award Number: 2016YFA0602301

## Abstract

Ecological responses to past climate change as determined from palaeorecords offer insights into responses that may accompany future climate change. In arid and semi-arid lands, the interactions between regional vegetation and climate change are not yet well understood, partly due to a lack of suitable palaeovegetation proxies that can provide accurate and continuous tracers for past vegetation dynamics. To gain a better understanding of long-term vegetation dynamics, this study employs a multiproxy approach applied to sand-palaeosol sediments of northeastern China's Songnen grasslands. Phytolith analyses and data on the stable carbon isotope composition ( $\delta^{13}\text{C}$ ) of organic matter are used to reconstruct palaeovegetation composition, namely, the changing abundance of C<sub>3</sub> and C<sub>4</sub> species, whereas a geochemical weathering index (Fed/Fet ratios) tracks past East Asian summer monsoon (EASM) intensity. The phytolith assemblages and indices and  $\delta^{13}\text{C}$  of the soil indicate that C<sub>4</sub> species' abundance has been increasing in the Songnen grasslands since the mid-Holocene, although C<sub>3</sub> vegetation is still dominant. Statistically significant negative correlations between the  $\delta^{13}\text{C}$  data and Fet/Fed ratios suggest that continuous weakening of the EASM since the mid-Holocene may be responsible for the  $^{13}\text{C}$ -enrichment of the

sediments in the Songnen grasslands. Field vegetation surveys, modern topsoil phytoliths and  $\delta^{13}\text{C}$  calibration data indicate that the expansion of C<sub>4</sub> species since the mid-Holocene is mainly due to their ability to cope with aridity when growing season temperature is not undergoing a significant decrease. Future precipitation decreases in arid and semi-arid lands should make C<sub>4</sub> species more competitive in the grasslands of northeastern China.

### Highlights

- A continuous grassland landscape history is reconstructed from a sand-palaeosol sequence via phytolith analysis.
- Multiple independent approaches were used to reconstruct past EASM intensity and palaeovegetation patterns.
- Phytolith and  $\delta^{13}\text{C}$  analyses indicate an increase in C<sub>4</sub> species since the mid-Holocene.
- Aridification drives the increase in C<sub>4</sub> species within the grassland ecosystem.

### KEY WORDS

C<sub>3</sub>/C<sub>4</sub> vegetation, East Asian summer monsoon, grasslands, mid-Holocene, northeastern China, phytolith

## 1 | INTRODUCTION

A better understanding of the interactions between climate change and vegetation dynamics of the past is critical for assessing how terrestrial vegetation ecosystems will respond to future climate change (Khon et al., 2014; Liu, Feng, et al., 2005; Liu, Huang, et al., 2005; Nelson, Hu, Tian, Stefanova, & Brown, 2004; Zhao, Yu, Chen, Zhang, & Yang, 2009; Zhao & Yu, 2012; Zhang, Zhao, Lu, & Faiia, 2003). In humid areas of East Asia, widely distributed lacustrine and peaty sediments recorded palaeoenvironment changes with a temporal resolution of a few years to several decades. Those sediments have provided excellent archives for evaluating the responses of vegetation to past climate variation (e.g., Stebich et al., 2015; Zhao et al., 2009 and references therein). Most investigations, however, point to complex interactions between climate change and vegetation ecosystems (e.g., Zhao et al., 2009; Zhao & Yu, 2012 and references therein), indicating that the response of vegetation to past climate change varied greatly in space and time. This emphasizes the importance of region-specific palaeoenvironmental change studies (Stebich et al., 2015; Zhao et al., 2009; Zhao & Yu, 2012). Therefore, regional vegetation dynamics induced by climate change, and associated feedback mechanisms, are still poorly understood, especially in arid and semi-arid environments (Zhao & Yu, 2012).

Arid and semi-arid lands cover about one-third of the world's land surface, including approximately one-third

of China (Yang et al., 2011). Vegetation in these areas is highly sensitive to precipitation and temperature variations (e.g., Li, Gao & Han, 2017; Zhao & Yu, 2012). Global climate changes are reportedly altering the relative abundances of C<sub>3</sub> and C<sub>4</sub> plants in these areas (Fox & Koch, 2003). For example, late Cenozoic grassland expansions are linked to climate change, especially when temperature decreases while aridity and seasonality increase (Fox & Koch, 2003; Osborne, 2008). However, geological evidence increasingly suggests that multiple environmental factors, including temperature, growing season precipitation, aridity, fire and atmospheric CO<sub>2</sub> concentration ( $p\text{CO}_2$ ), could change the natural abundance of C<sub>3</sub> and C<sub>4</sub> plants (Khon et al., 2014; Liu, Huang, et al., 2005; Rao et al., 2017; Zhang et al., 2003). The relative importance of these environmental factors, nevertheless, is widely debated (e.g. Ghosh, Sanyal, & Kumar, 2017; Khon et al., 2014; Liu, Feng, et al., 2005; Liu, Huang, et al., 2005; Ning, Liu, & An, 2008; Rao et al., 2017; Sun, Liu, Sun, & An, 2015; Vidic & Montañez, 2004; Zhang et al., 2003), forcing a reconsideration of the climate effects on C<sub>3</sub>/C<sub>4</sub> dominance.

Understanding past vegetation dynamics in arid and semi-arid landscapes has been hampered by the lack of suitable palaeovegetation proxies (Liu, Huang, et al., 2005; Nelson et al., 2004). Erosive and permanently aerobic conditions in arid and semi-arid lands prevent the preservation of most microfossils in the sediments (e.g., Alexandre, Meunier, Lézine, Vincens, & Schwartz, 1997; Barboni, Bonnefille, Alexandre, & Meunier, 1999;

Boyd, 2005). Many important palaeovegetation proxies, like pollen, charcoal, macrofossils and other fossil assemblages, are poorly preserved and thus present in very low concentrations in sandy sediments (Boyd, 2005), which are common in these climatic regions. Identifying suitable site-specific proxies and the use of multiple proxies are critical for the reliable reconstruction of palaeovegetation in arid and semi-arid environments (Li et al., 2018; Liu, Huang, et al., 2005; Nelson et al., 2004).

Phytoliths hold great promise for investigating the palaeovegetation dynamics in grasslands, not only because they bear morphological characteristics at the subfamily level of Poaceae (Barboni et al., 1999; Boyd, 2005; Bremond et al., 2008; Hyland, Sheldon, Smith, & Strömberg, 2018; Strömberg, 2004; Strömberg, Di Stilio, & Song, 2016; Twiss, Suess, & Smith, 1969; Twiss, 1992), but also because they can be well preserved in oxidizing conditions (Piperno, 1988; Wang & Lu, 1993). Compared with pollen, which is rarely found in sandy layers (e.g. Li, 1991; Qiu, Li, & Xia, 1992), phytoliths can provide continuous *in situ* records of palaeovegetation in arid regions, where conventional pollen analysis is not an option (Li et al., 2018). In addition to using phytoliths for palaeoecological investigations, occlusion of carbon within phytoliths is considered to be an important long-term terrestrial biogeochemical carbon sequestration mechanism and might play a significant role in mitigating climate change (Song, McGrouther, & Wang, 2016). Soils inherit the organic carbon isotopic composition of plants with little or negligible fractionation (Feng et al., 2008; Liu, Huang, et al., 2005; Rao et al., 2017; Sage, Wedin, & Li, 1999; Sun et al., 2015). Surface soil  $\delta^{13}\text{C}$  data faithfully reflect the  $\delta^{13}\text{C}$  values of the corresponding overlying vegetation, and variations in sedimentary  $\delta^{13}\text{C}$  at least partially demonstrate a change in vegetation cover (Rao et al., 2017). Thus, the  $\delta^{13}\text{C}$  signature of sediment organic matter is a good indicator of the dominance of C<sub>3</sub> versus C<sub>4</sub> plants through time, which are indirectly linked to temperature and precipitation (Liu, Huang, et al., 2005; Nelson et al., 2004; Rao et al., 2017; Silva et al., 2011).

Located at the eastern margin of the Eurasian steppes belt (also known as the Great Steppe), the Songnen grasslands are dominated by various Poaceae species and are one of the most important areas for food production and environmental security in China (Wang, Gao, & Chen, 2003). Sandy sediments and palaeosols are widely distributed in the grasslands (Li, 1991; Qiu et al., 1992). Like the loess-palaeosol sequences of the Chinese Loess Plateau, the study of which has led to significantly improved knowledge about Late Cenozoic climate evolution (e.g., Ding, Yang, Sun, & Liu, 2001; Guo et al., 2000; Lu et al., 2013), sand-palaeosol sequences in north China are also excellent continental archives that have been used to

help reconstruct the region's late Quaternary climate variations (e.g., Chen, Lu, et al., 2015; Guo et al., 2018; Yang et al., 2011). However, because the sandy layers in the grasslands lack sufficient extractable pollen, as well as other suitable palaeovegetation proxies, few studies have addressed the area's palaeovegetation dynamics and the potential climate forcing for grasslands vegetation change (Li, 1991; Qiu et al., 1992). This paper uses multiple, independent proxies from the sand-palaeosol sediments of the Songnen grasslands to reconstruct the region's Holocene palaeoclimate and palaeovegetation dynamics and to evaluate whether natural climate fluctuations during that epoch had a significant effect on grassland ecosystems. Combining stable carbon isotope and phytolith analyses provides an improved reconstruction of the regional palaeovegetation change and distribution patterns since the mid-Holocene. This research also uses geochemical weathering indices, modern field vegetation surveys, and phytolith and carbon isotope calibrations to refine the understanding of regional vegetation dynamics and their controlling factors.

## 2 | MATERIALS AND METHODS

### 2.1 | Regional setting

The Songnen grasslands (44°45'–48°20'N, 120°40'–126°00'E) are situated at the eastern margin of the Eurasian steppe belt (Figure S1) at an elevation of approximately 130 to 160 m (Xiao, 1995). It is a transitional belt between the agricultural region and the pastoral region. The climate of the Songnen grasslands is mainly influenced by the East Asian monsoon system, which has distinct seasonal variability. Seasons alternate between dry and windy springs, humid and warm summers with intensive rainfall, windy and dry autumns, and long, cold dry winters (Zhang et al., 2003). In winter, the dominant northwesterly winds bring dry and cold air masses to the region from the Eurasian continental interior. Summers are dominated by warm and humid air masses transported by southeasterly winds from the Pacific Ocean. Over this extensive area, average annual precipitation varies west to east from 360 mm to 480 mm. From north to south, average annual temperature over the Songnen grassland increases from 3.5°C to 5.0°C, with the lowest mean monthly temperatures in January (−22 to −18°C) and the highest in July (20 to 22°C) (Hou, 1988). Typically, 60–80% of the annual precipitation, which averages about 420 mm, falls during the growing season (from May to August) (Figure S1). The evaporation rate for this region increases from 1,200–1,600 mm/year in the east to 1,500–1,900 mm/year in the west. The frost-free period of

the study area is 130–165 days/year (Wang et al., 2009). The main rivers flowing through the study area are the Nunkiang, Songhua, Tao'er and Huolin Rivers. Alluvial and lacustrine sediments are the main components of Quaternary sediments in the Songnen plain (Li, 1991; Qiu et al., 1992).

The widespread sand found in the Songnen grasslands was transported by the wind from nearby alluvial and lacustrine sources (Li, 1991; Qiu et al., 1992). Aeolian sand and sandy dunes are common on the broad terraces of the Songhua (Song) and Nunkiang (Nen) Rivers within the grasslands (Figure S2A, Li, 1991; Qiu et al., 1992; Xiao et al., 1995). In the modern landscape of the Songnen grasslands, the paired ridge and swale landforms are common in the sandy terrain (Xiao et al., 1995). Soil types vary with local sub-environments. Kastanozem, Chernozems and Arenosols occur on the high plains and dunes, whereas Umbrisols, Solonchaks and Solonetz soils are found in the lowlands (Hou, 1988). Vegetation of the Songnen grasslands today is dominated by Poaceae and Compositae species, such as *Leymus chinensis*, *Filifolium sibiricum* and *Stipa baicalensis* (Hou, 1988). The main Poaceae species, their photosynthetic pathways, leaf  $\delta^{13}\text{C}$  values and habitats are listed in Table S1.

## 2.2 | Field sampling and chronology

In the summer of 2015, a complete 2.25-m deep sand-palaeosol section (section DK) was described and sampled in Tailai County, Heilongjiang Province, China. Two palaeosol layers between three sandy layers were observed within the section (Figure S1), each representing a relatively stable stage when vegetation covered the sandy sediments. The shallow and limited development of the palaeosols indicates that they formed during relatively short intervals of wetter climate within the overall period of accumulation of the sandy sediments (Figure S1C). The vegetation information recorded in the sandy-palaeosol materials is representative of the palaeovegetation that existed during the formation of the sandy lands (Figure S2). Sediment samples were collected at 5-cm intervals throughout the 2.25-m exposure, except between depths of 185 to 225 cm, which were sampled at 10-cm intervals because of their uniform nature. The 5-cm (or 10-cm) sediment sections were homogenized and prepared for further analysis. A total of 41 samples were collected and analysed for each proxy.

Based on sedimentary characteristics and stratigraphic units, four sediment samples were prepared for radiocarbon dating from bulk organic carbon. For sample preparation, any visible roots and other extraneous organic material were removed. Further, samples were treated with 0.1 N HCl for 1–2 hr, and washed free of

acid with Milli-Q water. After drying and homogenization, carbon in the pretreated samples was combusted into CO<sub>2</sub> and converted to graphite by reduction. The graphite samples were analysed for <sup>14</sup>C activity with a 250 keV single stage accelerator mass spectrometry (National Electrostatics Corporation, Middleton, Wisconsin) at Beta Analytic Inc. (Miami, Florida). Both the HCl pretreatment and <sup>14</sup>C measurements were conducted by Beta Analytic Inc.

The accelerator mass spectrometry (AMS) radioactive measurement for each sample was given in conventional years before present (yr BP) and calibrated into calendar years (cal. yr BP) from the IntCal13 calibration curve (Reimer et al., 2013) using the CALIB Rev. 7.04 program and expressed with 2 $\sigma$  ranges (Stuiver & Reimer, 1993). The chronologies were estimated with the Bacon v2.2 model (Blaauw & Christen, 2011).

## 2.3 | Laboratory methods

Phytoliths were extracted from 20-g subsamples of each of the 41 sediment samples using a modified version of the Piperno (1988) method (Wang & Lu, 1993). Each sub-sample was treated with 10% HCl to remove carbonates. Organic matter was removed using 10% H<sub>2</sub>O<sub>2</sub> at 70°C. Phytoliths were extracted through heavy liquid (ZnBr<sub>2</sub>) flotation at a density of 2.35 g/cm<sup>3</sup>. A tablet of *Lycopodium* spores (27,560 spores per tablet) was added to determine relative abundance of phytoliths (expressed as phytolith concentration in this study). After cleaning, each sample was rinsed in distilled water and ethanol and placed on slides in Canada balsam with a refractive index of 1.5216–1.5240 for counting and storage. Phytoliths were identified mainly following the classification system used by Lu et al. (2006), and with reference to the classification systems of Twiss et al. (1969). Phytolith identification, photographing and counting (usually >300 diagnostics per sample) were performed at  $\times 600$  magnification using an Olympus BX53 optical microscope (Olympus Corporation, Tokyo, Japan) at Northeast Normal University. Phytoliths were named according to the International Code for Phytolith Nomenclature 1.0 (Madella, Alexandre, & Ball, 2005).

For stable carbon isotope analyses, visible modern organic materials (e.g., roots) were first removed. All of the samples were then treated with 1 N HCl to remove carbonates. Decarbonization of the samples lasted for at least 24 hr, after which the residuals were rinsed with milli-Q water until the pH reached 7. Samples were dried at 65°C and homogenized before being loaded into tin capsules for isotopic analysis. The prepared samples were combusted into CO<sub>2</sub> in a Thermo Scientific Flash 2000 HT

elemental analyser (Thermo Fisher Scientific Inc., Waltham, MA) and then introduced into a Thermo Finnigan MAT 253 mass spectrometer (Thermo Finnigan LLC, San Jose, CA) at the National Research Center of Geoanalysis, Chinese Academy of Geological Sciences, to determine the  $^{13}\text{C}/^{12}\text{C}$  ratio. Organic carbon  $^{13}\text{C}/^{12}\text{C}$  ratios of each sample were reported as  $\delta^{13}\text{C}$ , in per mil (‰) versus PDB (Pee Dee Belemnite). Analytical uncertainty on  $\delta^{13}\text{C}$  measurements was  $<0.1\text{‰}$ , and replicate analyses yielded a mean standard deviation smaller than  $0.45\text{‰}$ .

The ratio (Fed/Fet) of citrate-bicarbonate-dithionite (CBD)-extractable iron (or free iron) to total iron concentrations has been suggested as a proxy for pedogenetic weathering degrees of the loess-palaeosol sequence, which is closely connected to the amount of monsoonal precipitation (Guo et al., 2000; Ding, Yang, Sun, & Liu, 2001). For analysis, the reactive Fe content (Fed, also known as free  $\text{Fe}_2\text{O}_3$ ) was extracted with citrate-bicarbonate-dithionite (CBD) solution from approximately 0.6 g of dry crushed samples using the method of Mehra and Jackson (1960). The extraction process was repeated at least three times until the solution became colourless. The total Fe content (Fet) for each sample was determined by dissolving approximately 0.5 g of the material in 10 ml HF, 10 ml  $\text{HNO}_3$  and 2 ml  $\text{HClO}_4$  mixed solution. Each sample was carefully digested for at least 12 hr at  $200^\circ\text{C}$  before 2 ml HCl was added to the residuals. Before measurement, hydroxylamine hydrochloride was used to reduce the  $\text{Fe}^{3+}$  into  $\text{Fe}^{2+}$  for all the extracted (or digested) samples. For colouration, a solution of 10-phenanthroline was added to each sample. Fed and Fet content were determined from the absorbance of the coloured sample solutions at the wavelength of 510 nm, based on calibration with a series of known-concentration Fe solutions (standards). The measurements were performed with an SP-722 Visible Spectrophotometer (Shanghai Spectrum Instruments Co., Ltd, Shanghai, China). Analytical precision for the absorbance measurements was 0.1%, whereas replicate analyses indicated mean standard deviations of 0.006% for Fed and 0.05% for Fet measurements.

The total organic carbon (TOC) and carbonate content were measured using a TOC analyser with a solid sample module (Aurora 1030 W TOC Analyzer, OI Scientific, College Station, TX). Dry and homogenized samples (approximately 800 mg each) were put into two individual small quartz boats after weighing. One was used for total carbon (TC) determination, whereas the other contained decarbonized samples for TOC measurements. All of the samples were combusted under  $\text{O}_2$  at a temperature of  $900^\circ\text{C}$ . The organic carbon was oxidized, inorganic carbon decomposed, and carbon content was calculated from the signals in the detector. The TOC content of the decarbonized samples was obtained in the same way. The inorganic carbon content of each sample was calculated by subtracting TOC from TC.

The grain-size distribution for each sample was determined using a MICROTAC S3500 laser particle-size analyser (Microtrac Inc., Montgomeryville, PA) with a measurement range of 0.02–2,000  $\mu\text{m}$  and an analytical error of less than 2%. The pretreatment procedure consisted of removing organic matter and carbonates with 10%  $\text{H}_2\text{O}_2$  and 10% HCl, respectively, followed by dispersal using 10 ml of 0.05 mol/L  $(\text{NaPO}_3)_6$  and treatment in an ultrasonic bath for 7 min. The texture composition for each sample is classified and named according to the Wentworth (1922) and Link (1966) sediment classification system.

All the above laboratory measurements were carried out at Northeast Normal University.

## 2.4 | Isotope mixing model and phytolith indices calculations

The abundance of  $\text{C}_3/\text{C}_4$  vegetation for each sample was inferred from carbon isotope compositions ( $\delta^{13}\text{C}_{\text{org}}$ ) using a two end-member mixing model (Vidic & Montañez, 2004). Assuming an average  $\delta^{13}\text{C}_{\text{org}}$  value of  $-13\text{‰}$  for  $\text{C}_4$  plants and  $-27\text{‰}$  for  $\text{C}_3$  plants,  $\text{C}_3$  and  $\text{C}_4$  plant percentages were calculated with the following isotope mass-balance equations (Vidic & Montañez, 2004):

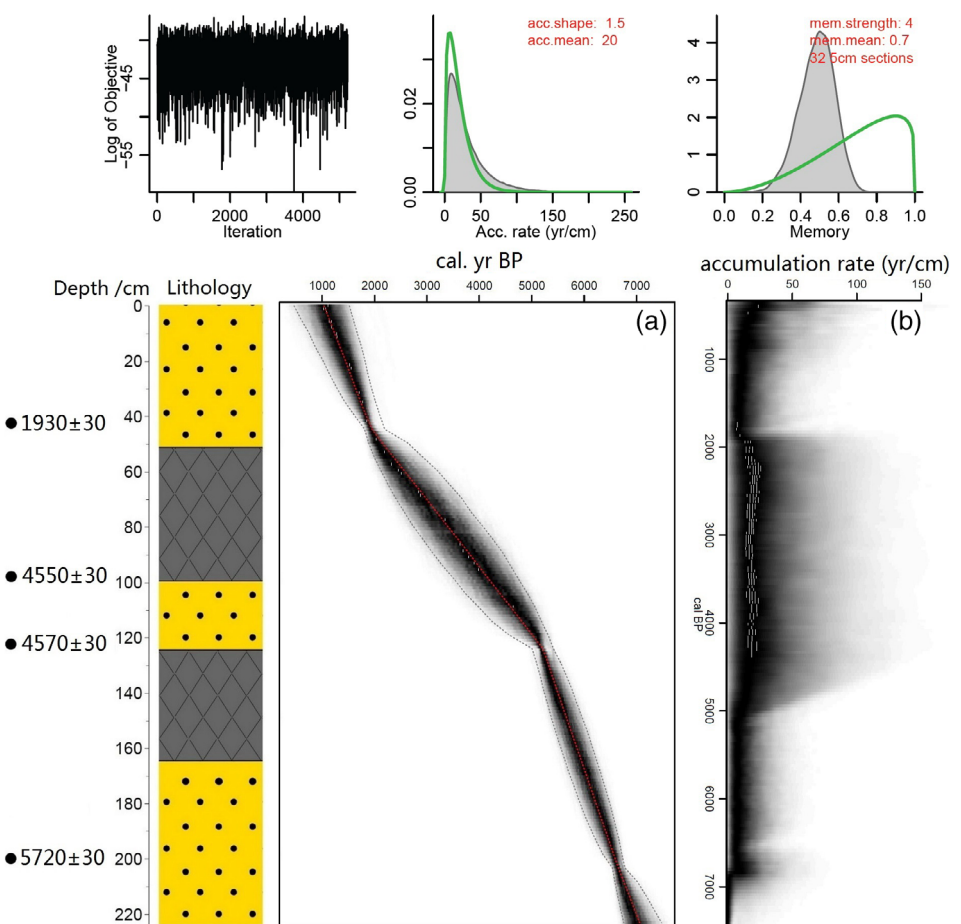
$$\text{C}_3(\%) = -(\delta^{13}\text{C}_{\text{org}} + 13) / (\delta^{13}\text{C}_{\text{C}4} - \delta^{13}\text{C}_{\text{C}3}) \times 100\%, \quad (1)$$

**TABLE 1** Accelerator mass spectrometry (AMS) radiocarbon dates of samples from the DK section

Sample ID	Depth (cm)	Laboratory code	Material	AMS $^{14}\text{C}$ BP	Uncertainty	2 $\sigma$ -range cal. BP <sup>a</sup>	Median age, cal. BP
DK9#	40–45	Beta-472977	Bulk organic matter	1,930	30	1,820–1,946	1,879
DK20#	95–100	Beta-472978	Bulk organic matter	4,550	30	5,053–5,317	5,159
DK25#	120–125	Beta-472979	Bulk organic matter	4,570	30	5,059–5,442	5,287
DK39#	195–205	Beta-472980	Bulk organic matter	5,720	30	6,415–6,631	6,508

<sup>a</sup>All ages were calibrated into calendar ages before present (BP) with the Intcal13 calibration data (Reimer et al., 2013) using the CALIB Rev. 7.04 program (Stuiver & Reimer, 1993).

**FIGURE 1** “Bacon” age-depth models (a) and accumulation rate plot (b) for the DK section. The best estimates for calibrated age are shown in red. The upper and lower estimates are shown in grey [Color figure can be viewed at [wileyonlinelibrary.com](http://wileyonlinelibrary.com)]



$$C_4(\%) = 100 - C_3(\%). \quad (2)$$

Phytolith indices  $I_c$  and  $I_{ph}$  values (Bremond et al., 2008) were calculated according to Twiss (1992) and Diester-Haass, Schrader, and Thiede (1973). The stratigraphic diagram was constructed using Tilia (Grimm, 1992).

### 3 | RESULTS

#### 3.1 | Chronological model

The calibrated ages reflect sample stratigraphic order within dating errors, without obvious inverted outliers (Table 1). Bacon-estimated chronologies for section DK suggest that the sequence recorded the palaeovegetation and palaeoclimate evolution in the Songnen grasslands from *ca.* 7,000 yr BP to 1,000 yr BP (Figure 1a). Palaeosol layers were formed during 5,900–5,200 cal. yr BP and 4,200–2,300 cal. yr BP. Accumulation rates from 5,000 yr to 2,000 yr are slower than in the other stages across the section, implying a period of vegetation increase due

to suitable climates and decreased wind blowing, whereas the relatively rapid accumulation rates during 7,000–5,000 yr and 2,000–1,000 yr BP (Figure 1b) are likely to be related to sand dune activities because of a drier and/or colder climate.

#### 3.2 | Grain size and geochemistry results

The sand-palaeosol section DK is dominated by sand (>63 µm), with the average sand content exceeding 85% (Figure 2). The sandy layers are composed of sand (more than 95%) and have no clay fraction; the palaeosol layers, in contrast, have some silt and clay. The mean grain size of the palaeosol sediments is about 176.1 µm, and it is about 194.4 µm for the sandy sediments (Figure 2).

Total organic carbon and inorganic carbon content (expressed as  $\text{CaCO}_3\%$  in Figure 2) show a similar pattern, having greater values in the palaeosols and smaller values in the sands. Likewise, free  $\text{Fe}_2\text{O}_3$  content (Fed%) is greater in the palaeosols than in the sands. Total iron (Fet%), however, varies little throughout the whole profile (Figure 2).

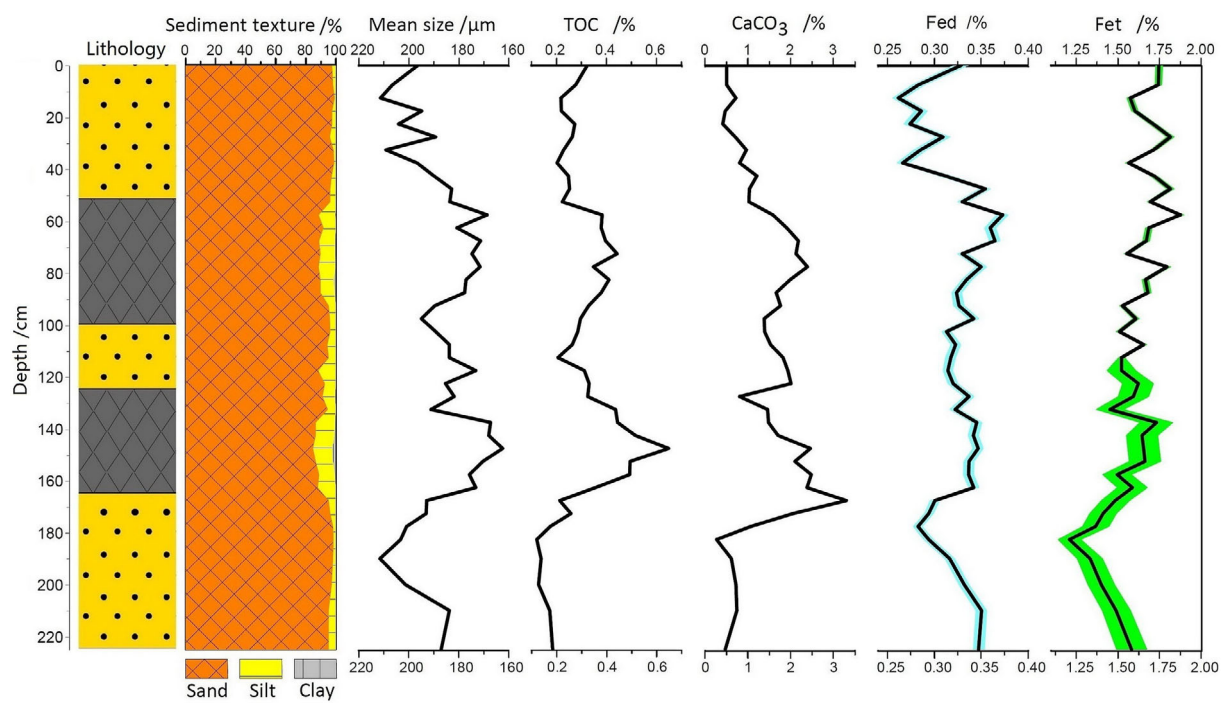


**FIGURE 2** Textural profile of section DK with selected geochemistry data plotted against depth. The blue and green shading represents measurement errors. TOC, total organic carbon [Color figure can be viewed at [wileyonlinelibrary.com](http://wileyonlinelibrary.com)]

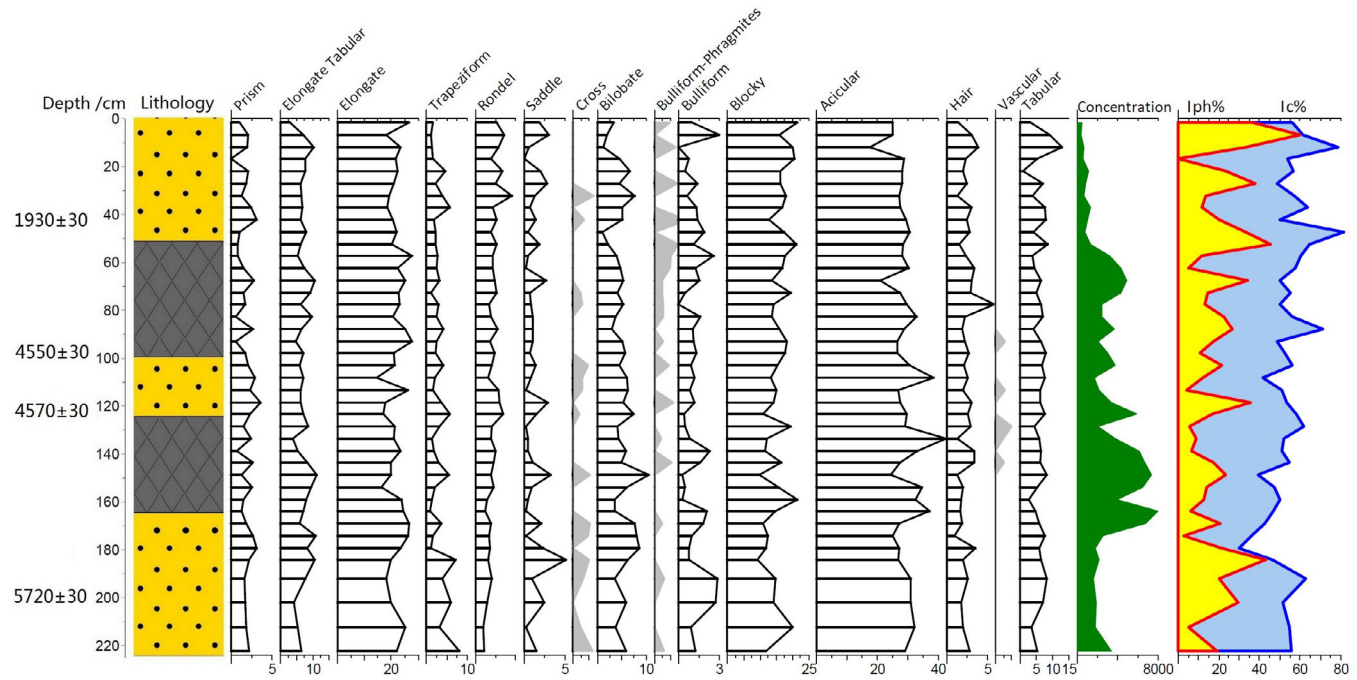


**FIGURE 3** Relative abundance of phytoliths (selected categories) observed in section DK and calculated phytolith indices. Exaggeration ( $\times 10$ ) is indicated by grey shading [Color figure can be viewed at [wileyonlinelibrary.com](http://wileyonlinelibrary.com)]

### 3.3 | Phytolith analysis and palaeoclimate reconstructions

The samples collected from section DK have an average phytolith abundance of approximately 3,000 grains per

gram of sediment. Morphotypes are diverse. Elongate and acicular types constitute more than 50% of the phytolith diagram for section DK (Figure 3). Trapeziform and rondel forms represent about 7% of the observed phytoliths, and bilobate phytoliths account for about 5%

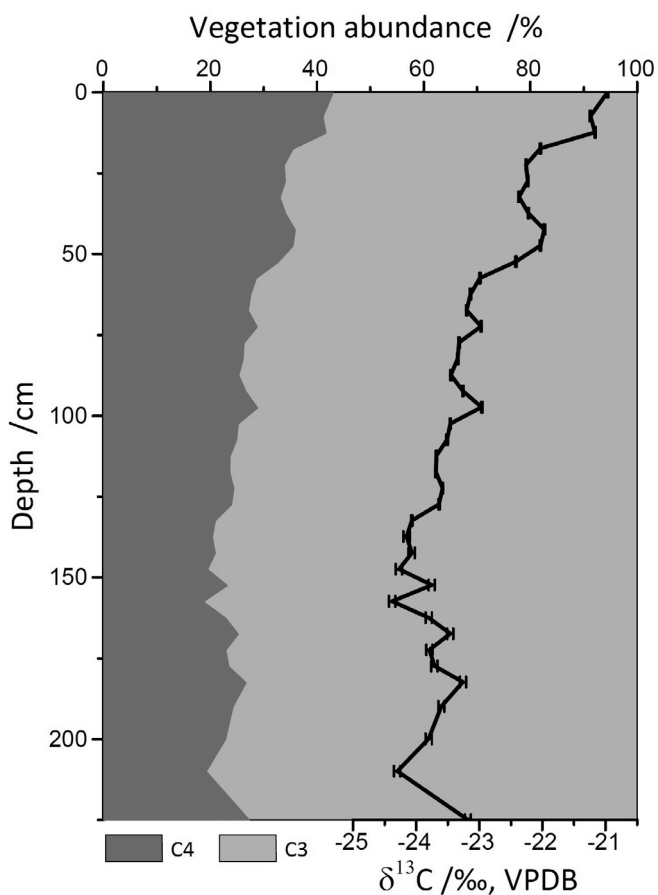


**FIGURE 4**  $C_3/C_4$  vegetation abundance reconstructions for section DK. Data show estimated relative abundance of  $C_3$  and  $C_4$  plants calculated from the isotopic mixing model (Vidic & Montañez, 2004) plotted against the depth. The solid line denotes the isotope profiles of section DK. VDPB, Vienna Pee Dee Belemnite

among all the samples. The saddle type of phytolith, typical of Chloridoideae, represents less than 2% on average through the section.

### 3.4 | Isotope composition and estimated $C_3/C_4$ abundance

The stable carbon isotopic composition of the sediments ( $\delta^{13}\text{C}_{\text{org}}$ ) ranges from  $-24.38\text{\textperthousand}$  to  $-20.97\text{\textperthousand}$  (mean =  $-23.14\text{\textperthousand}$ ,  $\sigma = 0.86\text{\textperthousand}$ ) for the whole section, with a tendency of gradual enrichment of  $\delta^{13}\text{C}_{\text{org}}$  from the base to the top of the section (Figure 4). Estimates of  $C_3/C_4$  abundance suggest a predominance of  $C_3$  plants, with  $C_3$  vegetation abundance ranging from 56.93% to 81.29% (mean = 72.42%,  $\sigma = 6.15\%$ ) and  $C_4$  abundance from 18.71% to 43.07% (mean = 27.58%,  $\sigma = 6.15\%$ ) throughout the section. Isotope analysis indicates that  $C_3$  plants have dominated the grasslands at least since

the mid-Holocene, but with  $C_4$  plants increasing over time (Figure 4). A *t*-test performed on the stable carbon isotope time series shows that this increasing trend from mid-Holocene to late Holocene is statistically significant ( $p < .001$ ).

## 4 | DISCUSSION

### 4.1 | Testing the reliability of phytolith and isotope signals

It has been argued that the transportation effects and the potential representation characteristics of phytoliths along a sedimentary section should be evaluated before using phytolith assemblages for palaeovegetation reconstruction (Fishkis, Ingwersen, Lamers, Denysenko, & Streck, 2010; Fishkis, Ingwersen, & Streck, 2009). Significant phytolith translocations will result in an enrichment of phytoliths in the lower part, and even to the base, of a section (Fishkis et al., 2009, 2010). The Songnen grassland site DK, however, lacks an obvious down-section accumulation of phytoliths (Figure 5). Likewise, smaller phytoliths that could more easily be translocated downward (e.g., acicular and rondel types) have not accumulated lower in the section (Figure 3). Even within each sand or palaeosol layer, no obvious enrichment of phytoliths is observed at the base of each unit (Figure 5a–d). Insignificant translocation of phytoliths is also supported by the positive correlation between phytolith concentration and TOC ( $r = 0.643$ ,  $p < .001$ ,  $N = 41$ , Figure S3). In addition, previous laboratory and field investigations reported a mean down-section phytolith translocation distance of  $2.20 \pm 0.10$  cm for a 6-month irrigation with 3,600 mm of water (Fishkis et al., 2010). Considering the 5-cm sampling resolution at section DK, it seems reasonable to conclude that negligible translocation occurs under the regional precipitation, which is less than 400 mm.

In modern soil profiles, the reduction of TOC content with depth is very common (e.g., Balesdent et al., 2018) and can be modelled as bicompartimental distributed carbon pools (Alexandre, Meunier, Mariotti, & Soubies, 1999; Balesdent et al., 2018). The bicompartimental model assumes that there are two pools of organic compounds. One pool is fed by the litter at the top of the profile and recycles rapidly, thus the organic carbon in that pool decreases with depth (Labile pool in Figure S4A). The second pool is more stable and translocation leads to a constant distribution with depth. At the base of a soil profile, therefore, nearly all of the organic carbon is from the stable pool (Figure S4A). The bicompartimental distribution of carbon pools in the soil profile results in a

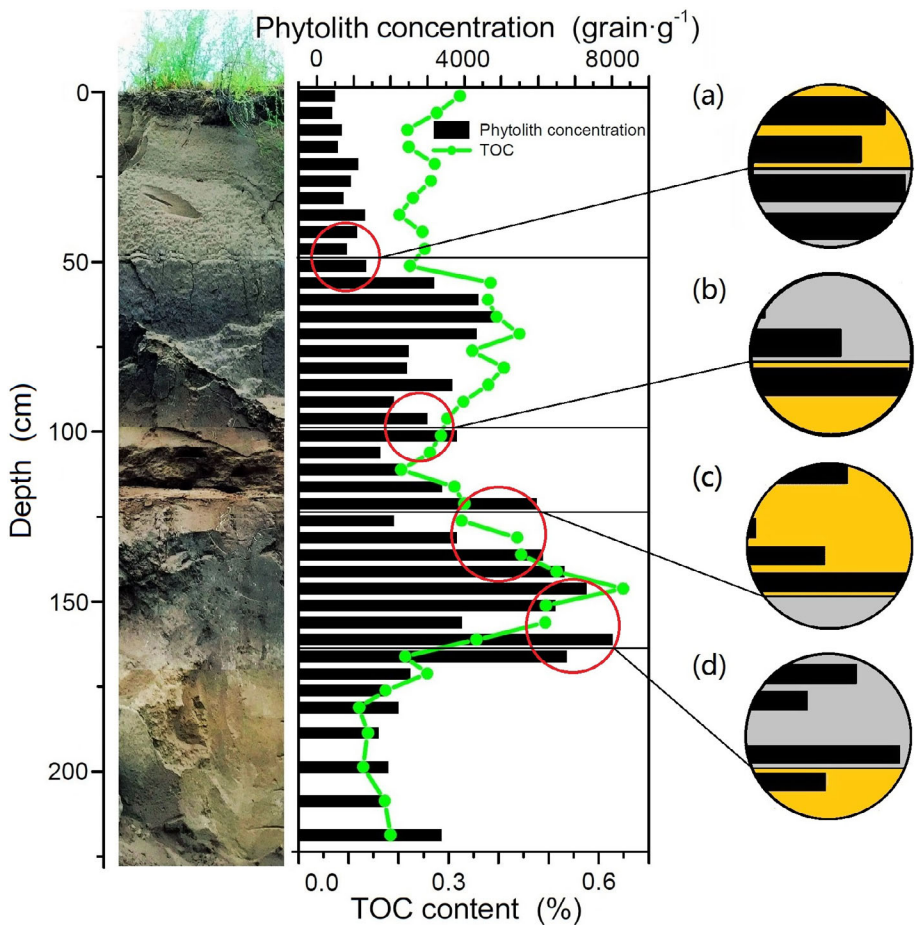


**FIGURE 5** Comparison of phytolith concentration and total organic carbon (TOC) profiles for section DK. (a)–(d) Phytolith concentration variations between different sedimentary units (e.g., sand-paleosol boundary) [Color figure can be viewed at [wileyonlinelibrary.com](http://wileyonlinelibrary.com)]

decrease in soil organic carbon concentration with depth that follows a natural logarithmic function (e.g., Balesdent et al., 2018; Boström, Comstedt, & Ekblad, 2007; Wynn, Harden, & Fries, 2006 and references therein, Figure S4B.①). At the same time, the isotopic composition of the TOC, due to kinetic fractionation during decomposition of organic carbon, will be enriched with depth (e.g., Alexandre et al., 1999; Boström et al., 2007; Wedin, Tieszen, Dewey, & Pastor, 1995; Wynn et al., 2006; Figure S4B.②). Because of the bicompartimental nature of the carbon pool, for palaeoclimate and palaeovegetation investigations, neither the natural decreasing trend of the TOC nor the natural enrichment of  $\delta^{13}\text{C}$  signals with depth could be interpreted as a shift in past vegetation dynamics (Alexandre et al., 1999; Wynn et al., 2006).

For section DK, however, neither the TOC profile (Figure 5) nor the  $\delta^{13}\text{C}_{\text{org}}$  profile (Figure 4) shows a bicompartimental distribution. The paleosol units yield a higher TOC content than the sandy layers (Figure 5), but even within the paleosols, the TOC and  $\delta^{13}\text{C}_{\text{org}}$  profiles do not indicate an obvious bicompartimental character. For example, in paleosol unit-1 (Figure S4B), the TOC content does not decrease logarithmically with depth

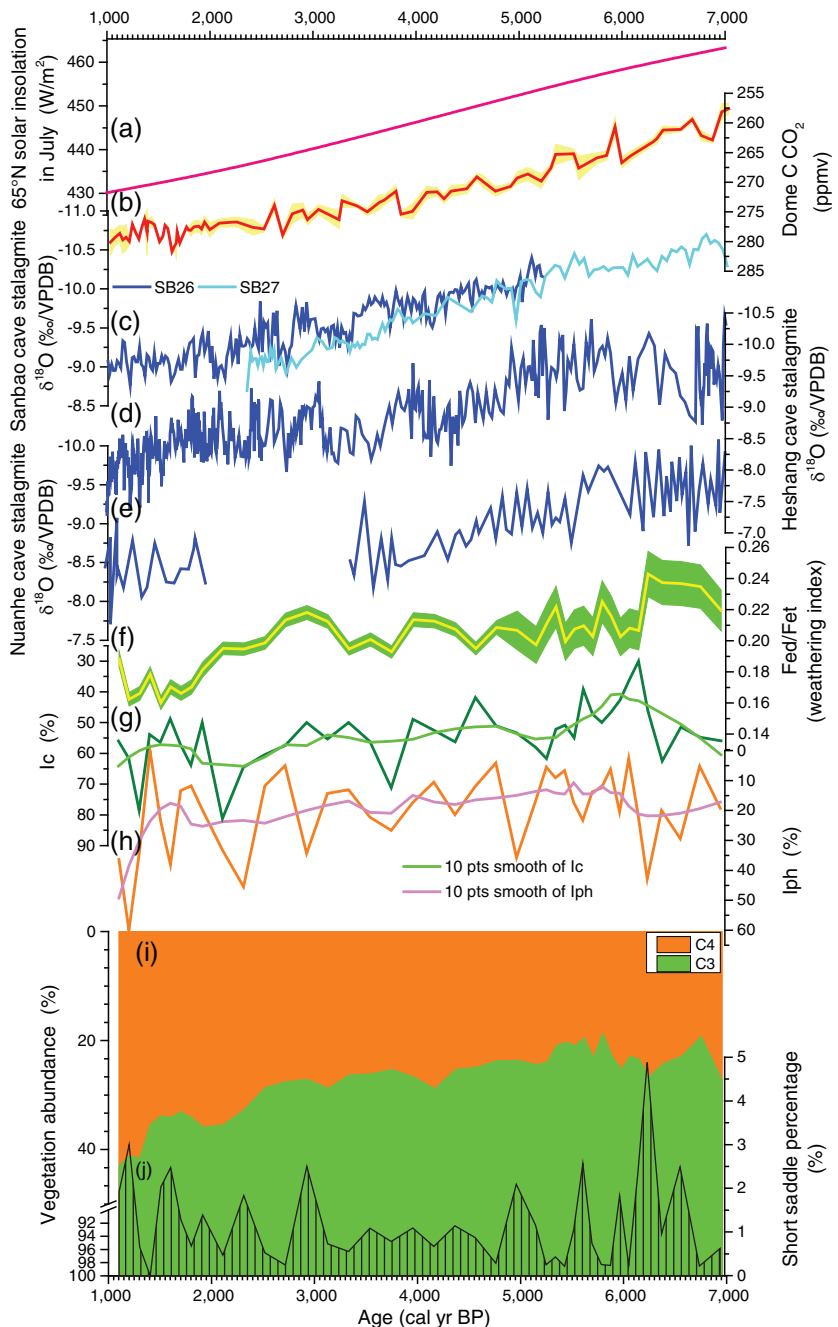
(green solid line in Figure S4B), nor does the  $\delta^{13}\text{C}_{\text{org}}$  trend show a logarithmic enriching trend (orange solid line in Figure S4B). In fact,  $\delta^{13}\text{C}_{\text{org}}$  gradually depletes from the top to the bottom of the section (Figure 4 and Figure S4), opposite from the logarithmic enrichment signal. Climate and/or vegetation shifts are likely to be responsible for the observed  $\delta^{13}\text{C}_{\text{org}}$  variations, which contrast with the bicompartimental distribution model.

In summary, the trends observed from these samples cannot be attributed to phytolith translocation effects and to bicompartimental distribution effects within the profile. Instead, the trends suggest that climate and/or vegetation variations have a significant influence on these profile characteristics.

#### 4.2 | Mid-Holocene C<sub>3</sub>/C<sub>4</sub> vegetation dynamics in Songnen grasslands and their link to EASM intensity

Topsoil phytolith assemblage calibrations in northeastern China have yielded a negative correlation between mean annual temperature (MAT, °C) and the Ic index, with a Pearson correlation coefficient  $r = -0.360$  ( $p < .001$ ,

**FIGURE 6** Comparisons of section DK multiproxy profiles with solar irradiation reconstructions, atmospheric CO<sub>2</sub> concentrations (in ppmv) and several absolutely dated stalagmite records in China. (a) Reconstructed Holocene solar irradiation at 65°N in July (Berger & Loutre, 1991); (b) reconstructed atmospheric CO<sub>2</sub> concentrations (MacFarling-Meure et al., 2006; Monnin et al., 2001, 2004; Rubino et al., 2013); (c) stalagmite δ<sup>18</sup>O records from Sanbao Cave, central China (Dong et al., 2010); (d) stalagmite δ<sup>18</sup>O records from Heshang Cave, central China (Hu et al., 2008); (e) stalagmite δ<sup>18</sup>O records from Nuanhe Cave, NE China (Wu, Wang, & Dong, 2011); (f) EASM-derived weathering index calculated as the ratio of Fed/Fet (this study); (g) phytolith assemblages calculated Ic index (this study); (h) phytolith assemblages calculated Iph index (i) δ<sup>13</sup>C estimated C<sub>3</sub> and C<sub>4</sub> abundances in the Songnen grasslands (this study); (j) percentages of short saddle phytoliths (this study). VDPB, Vienna Pee Dee Belemnite [Color figure can be viewed at wileyonlinelibrary.com]



N = 200) (Liu, 2017a). After analysing 83 topsoil phytolith assemblages along a precipitation gradient across northeastern China, Liu (2017b) also reported a negative correlation ( $r = -0.437$ ,  $p < .001$ ,  $N = 83$ ) between Iph and mean annual precipitation (MAP, mm). Thus, previous investigations provide evidences that both the Ic and Iph indices are valid in northeastern China and can be used to estimate regional palaeoclimate parameters (Liu, 2017a, 2017b).

In section DK, the Ic and Iph values show a general increasing trend from the mid- to late Holocene, with a co-varying character (Figure 6g,h). These phytolith index profiles suggest a decreasing trend in both palaeo-temperature

and palaeo-precipitation, implying a continuous weakening of EASM intensity since the mid-Holocene. The carbon isotope-based estimates of C<sub>3</sub>/C<sub>4</sub> species abundances show a decreasing trend of C<sub>3</sub> plant abundance and a relative expansion of C<sub>4</sub> plants (Figure 6i), reflected by the general enrichment of the δ<sup>13</sup>C<sub>org</sub> compositions. This slight C<sub>4</sub> expansion trend is also evidenced by an increasing content of the short saddle phytolith (Figure 6j), a diagnostic phytolith type (Figure S5) for Chloridoideae (C<sub>4</sub> plants), which has physiological advantages for coping with aridity in grasslands.

The Fed/Fet ratio displays an obvious decreasing trend from the bottom to the top of section DK (Figure 6f). The

Fed/Fet ratio peaked approximately 7,000–6,200 cal. yr BP, decreased sharply around 6,200 cal. yr BP, and then varied with a general decreasing trend (Figure 6f). The Fed/Fet profile agrees well with the variations of the stalagmite  $\delta^{18}\text{O}$  curves from Sanbao (Figure 6c; Dong et al., 2010) and Heshang Cave (Figure 6d; Hu et al., 2008) in central China (Figure 6c; Dong et al., 2010; Figure 6d; Hu et al., 2008) and Nuanhe Cave in northeastern China (Figure 6e; Wu et al., 2011), indicating that the ratio of Fed/Fet is a valid index to track past EASM intensity in the sandy lands. The increasing abundance of C<sub>4</sub> plants is almost synchronous with the Fed/Fet profile and stalagmite  $\delta^{18}\text{O}$  curves (Hu et al., 2008; Dong et al., 2010; Wu et al., 2011).

Modern C<sub>4</sub> plants occupy a wider range of drier and warmer habitats than C<sub>3</sub> plants because the C<sub>4</sub> pathway represents a pre-adaptation to hot and arid conditions (Silva et al., 2011; Rao et al., 2017). Under higher temperatures and increasing aridity, C<sub>4</sub> plants are more competitive than C<sub>3</sub> plants (Silva et al., 2011; Rao et al., 2017). In monsoonal Asia, mid- to late Holocene climate deterioration has been evidenced not only by aeolian sediments (e.g., Lu et al., 2013) and stalagmite data (e.g., Hu et al., 2008; Dong et al., 2010; Wu et al., 2011) but also by lacustrine (e.g., Chen, Xu, et al., 2015; Fan et al., 2016) and peat records (e.g., Li, Chambers, et al., 2017). In the present study, it appears that the weakening EASM intensity first caused a decrease in the regional precipitation that resulted in the shortage of available soil water (Yang et al., 2011). Because of their enhanced water-use efficiency, C<sub>4</sub> plants then became more competitive than C<sub>3</sub> plants (Khon et al., 2014; Liu, Huang, et al., 2005; Nelson et al., 2004).

#### 4.3 | The role of aridity in regulating C<sub>3</sub>/C<sub>4</sub> dynamics in the Songnen grasslands

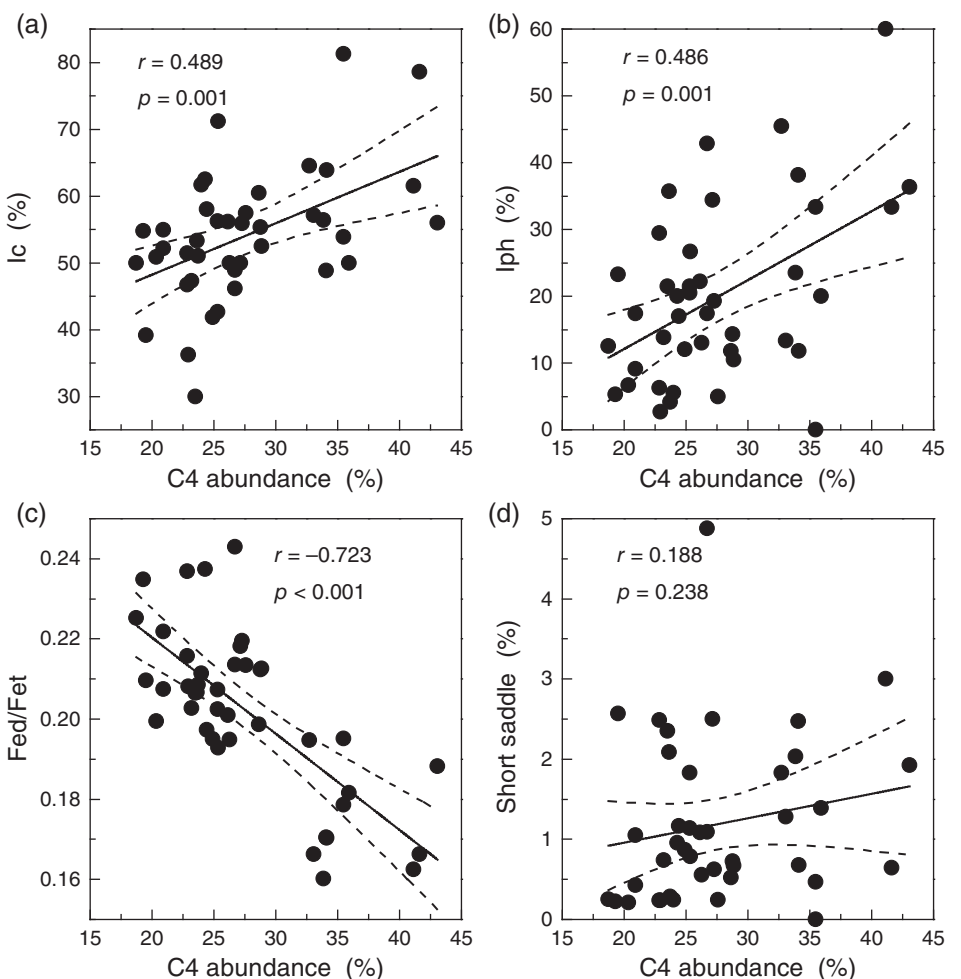
In the semi-humid and semi-arid Chinese Loess Plateau, almost all available data show that  $\delta^{13}\text{C}_{\text{org}}$  of palaeosols that developed during interglacials is more enriched (positive) than that of the loess (e.g., Liu, Feng, et al., 2005; Liu, Huang, et al., 2005; Ning et al., 2008; Sun et al., 2015; Vidic & Montañez, 2004; Zhang et al., 2003), suggesting C<sub>3</sub>-dominated loess intervals and a C<sub>3</sub>/C<sub>4</sub> vegetation mixture during the palaeosol intervals (Sun et al., 2015; Rao et al., 2017). C<sub>4</sub> plants occur/expand synchronously with a warm and humid interglacial climate, which was associated with changes in monsoon circulation (Liu, Feng, et al., 2005; Liu, Huang, et al., 2005; Ning et al., 2008; Rao et al., 2017; Sun et al., 2015; Vidic & Montañez, 2004; Zhang et al., 2003). Expansion of C<sub>4</sub> vegetation in the Chinese Loess Plateau occurred during

the intensified EASM (interglacial) stage and decreased during the weakened EASM (glacial) stages (e.g., Liu, Feng, et al., 2005; Liu, Huang, et al., 2005; Ning et al., 2008; Sun et al., 2015; Vidic & Montañez, 2004; Zhang et al., 2003).

In the Songnen Grasslands, which share a similar regional semi-humid and semi-arid climate with the Chinese Loess Plateau, the role of climate variables in influencing sediment  $\delta^{13}\text{C}_{\text{org}}$  signals seems different (Chen, Lu, et al., 2015; Guo et al., 2019). Topsoil calibrations across sandy lands in northeastern China revealed a significant negative correlation (Figure S6) between the  $\delta^{13}\text{C}_{\text{org}}$  signals and MAP ( $r = -0.721$ ,  $p < .001$ ,  $N = 90$ ), suggesting that precipitation controls the  $\delta^{13}\text{C}_{\text{org}}$  signature in the sandy lands (Chen, Lu, et al., 2015). Negative correlations between  $\delta^{13}\text{C}_{\text{org}}$  signals and MAP, as well as with aridity indices, have been confirmed by a recently published meta-data analysis carried out across several deserts in northeastern China (Guo et al., 2019). Considering the negative correlations (Liu, Feng, et al., 2005) between the  $\delta^{13}\text{C}$  of C<sub>3</sub> and C<sub>4</sub> plants and MAP for the Chinese Loess Plateau ( $-1.1\text{‰}/100 \text{ mm}$  for *Stipa bungeana* and  $-0.61\text{‰}/100 \text{ mm}$  for *Bothriochloa ischaemum*, respectively), Chen, Lu, et al. (2015) attributed the negative correlation between  $\delta^{13}\text{C}_{\text{org}}$  and MAP to the drier climate, which increased the  $\delta^{13}\text{C}$  values of C<sub>3</sub> plants, rather than to the variation of C<sub>3</sub>/C<sub>4</sub> biomass: because of the dominant contribution of C<sub>3</sub> plants to modern vegetation biomass in sandy lands, the drier climate introduced plant  $\delta^{13}\text{C}$  enrichments that will enrich the sandy sediments'  $\delta^{13}\text{C}_{\text{org}}$  (Chen, Lu, et al., 2015). To some extent, this assumption (Chen, Lu, et al., 2015) may explain the  $\delta^{13}\text{C}$  enrichment observed in the profile studied here. However, considering that the enrichment increment is about 1.1‰ per 100 mm (MAP) (Liu, Feng, et al., 2005), the 3.4‰  $\delta^{13}\text{C}$  differences across the profile (from  $-24.38\text{‰}$  to  $-20.97\text{‰}$ ) cannot be explained simply by the climate-introduced  $\delta^{13}\text{C}$  enrichments without robust supporting evidence.

According to Rao et al. (2017), topsoil  $\delta^{13}\text{C}$  values  $\leq -24\text{‰}$  can be assumed to form under pure C<sub>3</sub> vegetation, whereas soil  $\delta^{13}\text{C}$  values  $> -24\text{‰}$  correspond to mixed C<sub>3</sub>/C<sub>4</sub> or pure C<sub>4</sub> vegetation. The  $\delta^{13}\text{C}$  values for section DK reveal that most of them (35 out of 41) are greater than  $-24\text{‰}$ , suggesting a mixed C<sub>3</sub>/C<sub>4</sub> vegetation cover since the mid-Holocene. Besides the climate-introduced  $\delta^{13}\text{C}_{\text{org}}$  enrichments, the enriching trend observed in the  $\delta^{13}\text{C}_{\text{org}}$  profile indicates an increase in C<sub>4</sub> plants over time in the Songnen grasslands (Figure 6). This trend is further proved by the positive correlation between the Iph values and the estimated C<sub>4</sub> abundance (Figure 7b). A significant positive correlation was found between the C<sub>4</sub> abundance and Iph values ( $r = 0.486$ ,

**FIGURE 7** Correlations between multiple proxies of section DK with estimated C<sub>4</sub> abundances in the Songnen grasslands, northeastern China. (a) Ic versus estimated C<sub>4</sub> abundances; (b) Iph versus estimated C<sub>4</sub> abundances; (c) Fed/Fet versus estimated C<sub>4</sub> abundances; (d) short saddle percentages versus estimated C<sub>4</sub> abundances



$p = .001$ ,  $N = 41$ , Figure 7b), underscoring the agreement between the phytolith-deduced C<sub>4</sub> abundances and the  $\delta^{13}\text{C}$ -estimated C<sub>4</sub> abundances. Correlations between the Ic ( $r = 0.489$ ,  $p = .001$ ,  $N = 41$ , Figure 7a) values and estimated C<sub>4</sub> abundances also confirmed the response of C<sub>4</sub> plants to phytolith-based climate indices. The strong negative correlation between the Fed/Fet ratio and the estimated C<sub>4</sub> abundances ( $r = -0.723$ ,  $p < .001$ ,  $N = 41$ , Figure 7c) suggests an unambiguous monsoon influence on the C<sub>4</sub> abundance in this study area. Moreover, there is also a weak positive correlation for short saddle phytoliths in section DK and the C<sub>4</sub> abundance ( $r = 0.188$ ,  $p = .238$ ,  $N = 41$ , Figure 7d). All of the available evidence, therefore, points to a continuous increase of C<sub>4</sub> plants in the Songnen grasslands as a response to mid-Holocene climate transformation.

Field vegetation surveys could also help interpret the influences of climate parameters on C<sub>3</sub>/C<sub>4</sub> distribution patterns in the Songnen grasslands (Tang, 1999; Wang, Yin, & Li, 1997). Global C<sub>4</sub> plant distributions suggest that a minimum threshold temperature of 22°C for the warmest month limits the growth and distribution of C<sub>4</sub> species (Collatz, Berry, & Clark, 1998). Because C<sub>4</sub>

species have various mechanisms to cope with drought (Farquhar, Ehleringer, & Hubick, 1989; Khon et al., 2014; Liu, Huang, et al., 2005; Nelson et al., 2004; O'Leary, 1981; Rao et al., 2017; Sage et al., 1999), C<sub>4</sub> plants can adapt to aridity better than C<sub>3</sub> plants do when the climate deteriorates (Figure S7 and Table S1). Research carried out in arid and semi-arid lands points to a stronger correlation between the MAP and  $\delta^{13}\text{C}$  signals, rather than with MAT (e.g., Chen, Lu, et al., 2015; Guo et al., 2019; Tang, 1999). Moreover, along a precipitation gradient in northeastern China, field vegetation surveys show that the C<sub>4</sub> abundances (presented in percentages) display a negative correlation with MAP (Figure S7), supporting the controlling role of precipitation in regulating the C<sub>4</sub> distribution pattern (Tang, 1999).

In East Asia, Holocene climate modelling has revealed a 1.5°C decrease in summer season temperature from 6 ka BP (Wu, Liu, Cheng, & Chen, 2014) to the present (22.4°C, summer temperature at Tailai station, 1981 to 2010 average). With the growing season temperature above the threshold value since the mid-Holocene (Wu et al., 2014), precipitation may become the main limiting factor that controls the distribution and

dynamics of C<sub>4</sub> plants. However, during the glacial and interglacial cycles, the situation is different. The summer temperature decreased as much as 7°C on the Chinese Loess Plateau during the Last Glacial Maximum (Zhang et al., 2003). This large decrease in growing season temperature is too harsh for the growth/expansion of C<sub>4</sub> plants (Zhang et al., 2003); even the *p*CO<sub>2</sub> and precipitation are less (Zhang et al., 2003). This implies that during different geological intervals, the factors controlling C<sub>3</sub>/C<sub>4</sub> abundances could vary among regions (Ghosh et al., 2017; Khon et al., 2014; Liu, Feng, et al., 2005; Liu, Huang, et al., 2005; Ning et al., 2008; Rao et al., 2017; Sun et al., 2015; Vidic & Montañez, 2004; Zhang et al., 2003). Interestingly, C<sub>4</sub> expansion accelerates from *ca.* 2.5 ka to 1 ka BP (Figure 6), which may correspond to humans increasing the changes in vegetation cover in northeastern China (Guo et al., 2018, 2019). Intensified agriculture and poor land-use practices (Guo et al., 2018, 2019) may have overlapped with climatic effects to alter C<sub>3</sub>/C<sub>4</sub> vegetation cover during the late Holocene.

In summary, this study of phytolith- and isotope-based palaeovegetation data and Fed/Fet-based palaeoclimate reconstructions supports the view that effective precipitation is most likely the main factor that has been controlling vegetation dynamics in the Songnen grasslands. Both the geological and physiological evidence confirm that the continuous aridification since the mid-Holocene is responsible for the variation of C<sub>3</sub>/C<sub>4</sub> abundance, as inferred from the phytolith and δ<sup>13</sup>C data. In the future, with the growing season temperature above the threshold value, a decrease in precipitation (water availability stress) could alter the relative performance of C<sub>3</sub> and C<sub>4</sub> species, possibly resulting in C<sub>4</sub> plants becoming more competitive than C<sub>3</sub> species in grasslands ecosystems (Ward, Tissue, Thomas, & Strain, 1999).

## 5 | CONCLUSIONS

Employing geochemical, stable carbon isotope and phytolith analyses, this study reconstructs details of grassland vegetation dynamics in northeastern China since the mid-Holocene, and relates them to climate change. Independent approaches were used to separately reconstruct palaeoclimate and palaeovegetation. The phytolith and stable carbon isotope analyses both point to an increase in C<sub>4</sub> abundance since the mid-Holocene. Fed/Fet ratios reveal a continued weakening of EASM, which agrees with high precision dated stalagmite records in monsoonal China. Statistically significant negative correlations between past EASM intensity and estimated C<sub>4</sub> abundance support the conclusion that Holocene climate deterioration (aridification) drove the expansion of C<sub>4</sub> vegetation in the grasslands. C<sub>4</sub> plants appear to be better

adapted to and are more competitive than C<sub>3</sub> plants in arid habitats because of their physiological advantage of being more tolerant of water stress, especially when there is no significant decrease in growing season temperature. This is further supported by modern field vegetation surveys and topsoil phytolith and δ<sup>13</sup>C<sub>org</sub> calibrations in northeastern China. In the future, with a decrease in precipitation in sandy lands, C<sub>4</sub> species should be more competitive in the grasslands of northeastern China.

## ACKNOWLEDGEMENTS

We wish to thank all of the colleagues who attended the 11th International Meeting on Phytolith Research, where we received valuable and insightful comments on the parts of this manuscript that were presented during the meeting. We give special thanks to Rand Evett (UC Davis), Marco Madella (ICREA), Alexandra Golyeva (Institute of Geography, RAS), Doris Barboni (CEREGE) and Houyuan Lu (IGG, CAS), who provided very kind suggestions that improved the manuscript. The manuscript also benefited greatly from the comments of Anne Alexandre (CEREGE) on an earlier draft. We thank Dr Shasha Liu, Xinhua Zhou and Jingjing Sun (School of Geographical Sciences, NENU), who helped Nannan Li during the analyses of Fed, Fet, TOC and carbonate content. Finally, we thank the Editor-in-Chief, Prof Jennifer Dungait, and two anonymous reviewers for suggestions and comments that greatly improved the manuscript. This work was financially supported by the National Natural Science Foundation of China (Grant No. 41771214, 41471164, 41971100) and the National Key Research and Development Project of China (Grant No. 2016YFA0602301).

## CONFLICT OF INTEREST

No conflict of interest exists in the submission of this manuscript and the manuscript is approved by all authors for publication.

## DATA AVAILABILITY STATEMENT

The data that support the findings of this study are available as supplementary materials to this article.

## ORCID

Nannan Li  <https://orcid.org/0000-0002-0993-6900>  
Dongmei Jie  <https://orcid.org/0000-0001-6470-8719>

## REFERENCES

- Alexandre, A., Meunier, J.D., Lézine, A.M., Vincens, A., & Schwartz, D. (1997). Phytoliths: Indicators of grassland dynamics during the late Holocene in intertropical Africa. *Palaeogeography, Palaeoclimatology, Palaeoecology*, 136, 213–229.
- Alexandre, A., Meunier, J.D., Mariotti, A., & Soubies, F. (1999). Late Holocene phytolith and carbon isotope record from a

- latosol at Salitre, South-Central Brazil. *Quaternary Research*, 51, 187–194.
- Balesdent, J., Basile-Doelsch, I., Chadoeuf, J., Cornu, S., Derrien, D., Fekiacova, Z., & Hatté, C. (2018). Atmosphere–soil carbon transfer as a function of soil depth. *Nature*, 559, 599–602.
- Barboni, D., Bonnefille, R., Alexandre, A., & Meunier, J. D. (1999). Phytoliths as paleoenvironmental indicators, West Side Middle Awash Valley, Ethiopia. *Palaeogeography, Palaeoclimatology, Palaeoecology*, 152, 87–100.
- Berger, A., & Loutre, M. F. (1991). Insolation values for the climate of the last 10 million years. *Quaternary Science Reviews*, 10, 297–317.
- Blaauw, M., & Christen, J. A. (2011). Flexible paleoclimate age-depth models using an autoregressive gamma process. *Bayesian Analysis*, 6, 457–474.
- Boström, B., Comstedt, D., & Ekblad, A. (2007). Isotope fractionation and  $^{13}\text{C}$  enrichment in soil profiles during the decomposition of soil organic matter. *Oecologia*, 153, 89–98.
- Boyd, M. (2005). Phytoliths as paleoenvironmental indicators in a dune field on the northern Great Plains. *Journal of Arid Environments*, 61, 357–375.
- Bremond, L., Alexandre, A., Wooller, M. J., Hély, C., Williamson, D., Schäfer, P. A., ... Guiot, J. (2008). Phytolith indices as proxies of grass subfamilies on East African tropical mountains. *Global and Planetary Change*, 61, 209–224.
- Chen, F., Xu, Q., Chen, J., Birks, J. H. B., Liu, J., Zhang, S., ... Rao, Z. (2015). East Asian summer monsoon precipitation variability since the last deglaciation. *Scientific Reports*, 5, 11186. <https://doi.org/10.1038/srep11186>
- Chen, Y., Lu, H., Zhang, E., Zhang, H., Xu, Z., Yi, S., & Wu, S.-Y. (2015). Test stable carbon isotopic composition of soil organic matters as a proxy indicator of past precipitation: Study of the sand fields in northern China. *Quaternary International*, 372, 79–86.
- Collatz, G. J., Berry, J. A., & Clark, J. S. (1998). Effects of climate and atmospheric  $\text{CO}_2$  partial pressure on the global distribution of C4 grasses: Present, past, and future. *Oecologia*, 114, 441–454.
- Diester-Haass, L., Schrader, H. J., & Thiede, J. (1973). Sedimentological and paleoclimatological investigations of two pelagic ooze cores off Cape Barbas, North-West Africa. *Meteor Forschungsergebnisse*, 16, 19–66.
- Ding, Z., Yang, S., Sun, J., & Liu, T. (2001). Iron geochemistry of loess and red clay deposits in the Chinese Loess Plateau and implications for long-term Asian monsoon evolution in the last 7.0 Ma. *Earth and Planetary Science Letters*, 185, 99–109.
- Dong, J., Wang, Y., Cheng, H., Hardt, B., Edwards, R. L., Kong, X., ... Zhao, K. (2010). A high-resolution stalagmite record of the Holocene East Asian Monsoon from Mt Shennongjia, central China. *The Holocene*, 20, 257–264.
- Fan, J., Xiao, J., Wen, R., Zhang, S., Wang, X., Cui, L., ... Yamagata, H. (2016). Droughts in the East Asian summer monsoon margin during the last 6 kyrs: Link to the North Atlantic cooling events. *Quaternary Science Reviews*, 151, 88–99.
- Farquhar, G. D., Ehleringer, J. R., & Hubick, K. T. (1989). Carbon isotope discrimination and photosynthesis. *Annual Review of Plant Physiology and Plant Molecular Biology*, 40, 503–537.
- Feng, Z., Wang, L., Ji, Y., Guo, L., Lee, X., & Dworkin, S. I. (2008). Climatic dependency of soil organic carbon isotopic composition along the S–N Transect from 34°N to 52°N in central-east Asia. *Palaeogeography, Palaeoclimatology, Palaeoecology*, 257, 335–343.
- Fishkis, O., Ingwersen, J., Lamers, M., Denysenko, D., & Streck, T. (2010). Phytolith transport in soil: A laboratory study on intact soil cores. *European Journal of Soil Science*, 61, 445–455.
- Fishkis, O., Ingwersen, J., & Streck, T. (2009). Phytolith transport in sandy sediment: Experiments and modelling. *Geoderma*, 151, 168–178.
- Fox, D. L., & Koch, P. L. (2003). Tertiary history of C4 biomass in the Great Plains, USA. *Geology*, 31, 809–812.
- Ghosh, S., Sanyal, P., & Kumar, R. (2017). Evolution of C4 plants and controlling factors: Insight from *n*-alkane isotopic values of NW Indian Siwalik paleosols. *Organic Geochemistry*, 110, 110–121.
- Grimm, E. C. (1992). *TILIA and TILIA\*GRAPH computer program*. Springfield, MA: Illinois State Museum.
- Guo, L., Xiong, S., Ding, Z., Jin, G., Wu, J., & Ye, W. (2018). Role of the mid-Holocene environmental transition in the decline of late Neolithic cultures in the deserts of NE China. *Quaternary Science Reviews*, 190, 98–113.
- Guo, L., Xiong, S., Dong, X., Ding, Z., Yang, P., Zhao, H., ... Zheng, L. (2019). Linkage between C4 vegetation expansion and dune stabilization in the deserts of NE China during the late Quaternary. *Quaternary International*, 503, 10–23.
- Guo, Z., Biscaye, P., Wei, L., Chen, X., Peng, S., & Liu, T. (2000). Summer monsoon variations over the last 1.2 Ma from the weathering of loess-soil sequences in China. *Geophysical Research Letters*, 27, 1751–1754.
- Hou, X. (1988). *Physical geography of China: Phytogeography*. Beijing, China: Science Press (in Chinese).
- Hu, C., Henderson, G. M., Huang, J., Xie, S., Sun, Y., & Johnson, K. R. (2008). Quantification of Holocene Asian monsoon rainfall from spatially separated cave records. *Earth and Planetary Science Letters*, 226, 221–232.
- Hyland, E. G., Sheldon, N. D., Smith, S. Y., & Strömborg, C. A. E. (2018). Late Miocene rise and fall of C4 grasses in the western United States linked to aridification and uplift. *Geological Society of America Bulletin*, 131(1–2), 224–234.
- Khon, V. C., Wang, Y. V., Krebs-Kanzow, U., Kaplan, J. O., Schneider, R. R., & Schneider, B. (2014). Climate and  $\text{CO}_2$  effects on the vegetation of southern tropical Africa over the last 37,000 years. *Earth and Planetary Science Letters*, 403, 407–417.
- Li, N., Chambers, F. M., Yang, J., Jie, D., Liu, L., Liu, H., ... Qiao, Z. (2017). Records of East Asian monsoon activities in Northeastern China since 15.6 ka, based on grain size analysis of peaty sediments in the Changbai Mountains. *Quaternary International*, 447, 158–169.
- Li, N., Sack, D., Gao, G., Liu, L., Li, D., Yang, X., ... Leng, C. (2018). Holocene *Artemisia*-*Chenopodiaceae*-dominated grassland in North China: Real or imaginary? *The Holocene*, 28(5), 834–841.
- Li, Q. (1991). A primary study on the historical change of Songnen Sandy Land. *Chinese Science Bulletin*, 36, 487–489.
- Li, Z., Gao, Y., & Han, L. (2017). Holocene vegetation signals in the Alashan Desert of northwest China revealed by lipid molecular

- proxies from calcareous root tubes. *Quaternary Research*, 88, 60–70.
- Link, A. G. (1966). Textural classification of sediments. *Sedimentology*, 7(3), 249–254.
- Liu, H. (2017a). *Research on the distribution of the phytolith in surface soil and the reconstruction of temperature-humidity pattern during the Holocene in Northeast China*. PhD thesis. Northeast Normal University, Changchun (in Chinese).
- Liu, L. (2017b). *Characteristics of phytolith transport and preservation of typical soils in Northeast China and its application for palaeoenvironmental reconstruction*. PhD thesis. Northeast Normal University, Changchun (in Chinese).
- Liu, W., Feng, X., Ning, Y., Zhang, Q., Cao, Y., & An, Z. (2005).  $\delta^{13}\text{C}$  variation of C3 and C4 plants across an Asian monsoon rainfall gradient in arid northwestern China. *Global Change Biology*, 11, 1094–1100.
- Liu, W., Huang, Y., An, Z., Clemens, S. C., Li, L., Prell, W. L., & Ning, Y. (2005). Summer monsoon intensity controls C4/C3 plant abundance during the last 35 ka in the Chinese Loess Plateau: Carbon isotope evidence from bulk organic matter and individual leaf waxes. *Palaeogeography, Palaeoclimatology, Palaeoecology*, 220, 243–254.
- Lu, H., Wu, N., Yang, X., Jiang, H., Liu, K., & Liu, T. (2006). Phytoliths as quantitative indicators for the reconstruction of past environmental conditions in China I: Phytolith based transfer functions. *Quaternary Science Reviews*, 25, 945–959.
- Lu, H., Yi, S., Liu, Z., Mason, J., Jiang, D., Cheng, J., & Otto-Btiesner, B. (2013). Variation of East Asian monsoon precipitation during the past 21 ky and potential CO<sub>2</sub> forcing. *Geology*, 41, 1023–1026.
- MacFarling-Meure, C., Etheridge, D., Trudinger, C., Steele, P., Langenfelds, R., van Ommen, T., ... Elkins, J. (2006). Law Dome CO<sub>2</sub>, CH<sub>4</sub> and N<sub>2</sub>O ice core records extended to 2000 years BP. *Geophysical Research Letters*, 33, L14810. <https://doi.org/10.1029/2006GL026152>
- Madella, M., Alexandre, A., & Ball, T. (2005). International code for phytolith nomenclature 1.0. *Annals of Botany*, 96, 253–260.
- Mehra, O. P., & Jackson, M. L. (1960). Iron oxide removal from soils and clays by a dithionite-citrate system buffered with sodium bicarbonate. *Clays and Clay Minerals*, 5, 317–327.
- Monnin, E., Indermühle, A., Dällenbach, A., Flückiger, J., Stauffer, B., Stocker, T. F., ... Barnola, J. M. (2001). Atmospheric CO<sub>2</sub> concentrations over the last glacial termination. *Science*, 291, 112–114.
- Monnin, E., Steig, E. J., Siegenthaler, U., Kawamura, K., Schwander, J., Stauffer, B., ... Fischer, H. (2004). Evidence for substantial accumulation rate variability in Antarctica during the Holocene, through synchronization of CO<sub>2</sub> in the Taylor Dome, Dome C and DML ice cores. *Earth and Planetary Science Letters*, 224, 45–54.
- Nelson, D. M., Hu, F. S., Tian, J., Stefanova, I., & Brown, T. A. (2004). Response of C3 and C4 plants to middle-Holocene climatic variation near the prairie-forest ecotone of Minnesota. *Proceedings of the National Academy of Sciences of the United States of America*, 101, 562–567.
- Ning, Y., Liu, W., & An, Z. (2008). A 130-ka reconstruction of precipitation on the Chinese Loess Plateau from organic carbon isotopes. *Palaeogeography, Palaeoclimatology, Palaeoecology*, 270, 59–63.
- O'Leary, M. H. (1981). Carbon isotope fractionation in plants. *Phytochemistry*, 20, 553–567.
- Osborne, C. P. (2008). Atmosphere, ecology and evolution: What drove the Miocene expansion of C4 grasslands? *Journal of Ecology*, 96, 35–45.
- Piperno, D. R. (1988). *Phytolith Analysis. An Archaeological and Geological Perspective*. New York, NY: Academic Press.
- Qiu, S., Li, Q., & Xia, Y. (1992). Paleosols of sandy lands and environmental changes in the western plain of Northeast China during Holocene. *Quaternary Science*, 3, 224–232 (in Chinese).
- Rao, Z., Guo, W., Cao, J., Shi, F., Jiang, H., & Li, C. (2017). Relationship between the stable carbon isotopic composition of modern plants and surface soils and climate: A global review. *Earth-Science Reviews*, 165, 110–119.
- Reimer, P. J., Bard, E., Bayliss, A., Beck, J. W., Blackwell, P. G., Bronk Ramsey, C., ... Richard A Staff. (2013). IntCal13 and Marine13 radiocarbon age calibration curves 0–50,000 yr cal BP. *Radiocarbon*, 55(4), 1869–1887.
- Rubino, M., Etheridge, D. M., Trudinger, C. M., Allison, C. E., Battle, M. O., & Langenfelds, R. L. (2013). A revised 1000 year atmospheric  $\delta^{13}\text{C}$  -CO<sub>2</sub> record from Law Dome and South Pole, Antarctica. *Journal of Geophysical Research: Atmospheres*, 118, 8482–8499.
- Sage, R. F., Wedin, D. A., & Li, M. (1999). The biogeography of C4 photosynthesis: Patterns and controlling factors. In R. F. Sage & R. K. Monson (Eds.), *C4 Plant Biology* (pp. 313–373). San Diego, CA: Academic Press.
- Silva, L. C., Giorgis, M. A., Anand, M., Enrico, L., Pérez-Harguindeguy, N., Falczuk, V., ... Cabido, M. (2011). Evidence of shift in C4 species range in central Argentina during the late Holocene. *Plant and Soil*, 349, 261–279.
- Song, Z., McGrath, K., & Wang, H. (2016). Occurrence, turnover and carbon sequestration potential of phytoliths in terrestrial ecosystems. *Earth-Science Reviews*, 158, 19–30.
- Stebich, M., Rehfeld, K., Schlütz, F., Tarasov, P. E., Liu, J., & Mingram, J. (2015). Holocene vegetation and climate dynamics of NE China based on the pollen record from Sihailongwan Maar Lake. *Quaternary Science Reviews*, 124, 275–289.
- Strömberg, C. A. E. (2004). Using phytolith assemblages to reconstruct the origin and spread of grass-dominated habitats in the Great Plains of North America during the late Eocene to early Miocene. *Palaeogeography, Palaeoclimatology, Palaeoecology*, 207, 239–275.
- Strömberg, C. A. E., Di Stilio, V. S., & Song, Z. (2016). Functions of phytoliths in vascular plants: An evolutionary perspective. *Functional Ecology*, 30, 1286–1297.
- Stuiver, M., & Reimer, P. J. (1993). Extended <sup>14</sup>C database and revised CALIB radiocarbon calibration program. *Radiocarbon*, 35, 215–230.
- Sun, B., Liu, W., Sun, Y., & An, Z. (2015). The precipitation “threshold values” on C4/C3 abundance of the Loess Plateau, China. *Science Bulletin*, 60, 718–725.
- Tang, H. (1999). Distribution of C4 plants along the Northeast China transect and its correlation to the environmental factors. *Chinese Science Bulletin*, 44, 1316–1320.
- Twiss, P. C. (1992). Predicted world distribution of C3 and C4 grass phytoliths. In G. R. Rapp & S. C. Mulholland (Eds.), *Phytoliths systematics: Emerging issues. Advance Archaeological Museum Science*, 1 (pp. 113–128). New York, NY: Plenum Press.

- Twiss, P. C., Suess, E., & Smith, R. M. (1969). Morphological classification of grass phytoliths. *Soil Science Society of America Journal*, 33, 109–115.
- Vidic, N. J., & Montañez, I. P. (2004). Climatically driven glacial-interglacial variations in C3 and C4 plant proportions on the Chinese Loess Plateau. *Geology*, 32(4), 337–340.
- Wang, P., Yin, L., & Li, J. (1997). Ecological distribution and physiological adaptation to saline-alkaline environment of C3 and C4 plants in Northeastern China prairie area. *Chinese Journal of Applied Ecology*, 8(4), 407–411 (in Chinese).
- Wang, R., Gao, Q., & Chen, Q. (2003). Effects of climatic change on biomass and biomass allocation in *Leymus chinensis* (Poaceae) along the North-east China Transect (NECT). *Journal of Arid Environments*, 54, 653–665.
- Wang, Y., & Lu, H. (1993). *The Study of Phytolith and its Application*. Beijing, China: China Ocean Press (in Chinese).
- Wang, Z., Song, K., Zhang, B., Liu, D., Ren, C., Luo, L., ... Liu, Z. (2009). Shrinkage and fragmentation of grasslands in the West Songnen Plain, China. *Agriculture, Ecosystems and Environment*, 129, 315–324.
- Ward, J. K., Tissue, D. T., Thomas, R. B., & Strain, B. R. (1999). Comparative responses of model C3 and C4 plants to drought in low and elevated CO<sub>2</sub>. *Global Change Biology*, 5, 857–867.
- Wedin, T. A., Tieszen, L. L., Dewey, B., & Pastor, J. (1995). Carbon isotope dynamics during grass decomposition and soil organic matter formation. *Ecology*, 76, 1383–1392.
- Wentworth, C. K. (1922). A Scale of Grade and Class Terms for Clastic Sediments. *The Journal of Geology*, 30(5), 377–392.
- Wu, J., Wang, Y., & Dong, J. (2011). Changes in East Asian summer monsoon during the Holocene recorded by stalagmite δ<sup>18</sup>O records from Liaoning Province. *Quaternary Science*, 31(6), 990–998 (in Chinese).
- Wu, P., Liu, Z., Cheng, J., & Chen, G. (2014). Simulation of spatial-temporal asynchronism of East Asian summer's surface-air temperature response to orbital forcing since the Mid-Holocene. *Chinese Journal of Geophysics*, 57(6), 1757–1768 (in Chinese).
- Wynn, J. G., Harden, J. W., & Fries, T. L. (2006). Stable carbon isotope depth profiles and soil organic carbon dynamics in the lower Mississippi Basin. *Geoderma*, 131, 89–109.
- Xiao, R. (1995). Geographical location and principle regional characteristics of desertification-prone lands of the Songnen Sandy Land. In R. Xiao (Ed.), *The Research on the Desertification of the Songnen Sandy Land in Northeast China* (pp. 1–8). Changchun, China: Northeast Normal University Press (in Chinese).
- Yang, X., Scuderi, L., Paillou, P., Liu, Z., Li, H., & Ren, X. (2011). Quaternary environmental changes in the drylands of China – a critical review. *Quaternary Science Reviews*, 30, 3219–3233.
- Zhang, Z., Zhao, M., Lu, H., & Faiia, A. M. (2003). Lower temperature as the main cause of C4 plant declines during the glacial periods on the Chinese Loess Plateau. *Earth and Planetary Science Letters*, 214, 467–481.
- Zhao, Y., & Yu, Z. (2012). Vegetation response to Holocene climate change in East Asian monsoon-margin region. *Earth-Science Reviews*, 113, 1–10.
- Zhao, Y., Yu, Z., Chen, F., Zhang, J., & Yang, B. (2009). Vegetation response to Holocene climate change in monsoon-influenced region of China. *Earth-Science Reviews*, 97, 242–256.

## SUPPORTING INFORMATION

Additional supporting information may be found online in the Supporting Information section at the end of this article.

**How to cite this article:** Li N, Xie M, Sack D, et al. Continuous aridification since the mid-Holocene as the main cause of C<sub>3</sub>/C<sub>4</sub> dynamics in the grasslands of northeastern China. *Eur J Soil Sci*. 2021;72:356–371. <https://doi.org/10.1111/ejss.12960>